CARBON 57 (2013) 274–281

Available at www.sciencedirect.com

SciVerse ScienceDirect

journal homepage: www.elsevier.com/locate/carbon

Nanoparticle decoration of carbon nanotubes by sputtering

C. Muratore [a,b,*], A.N. Reed [b], J.E. Bultman [b,c], S. Ganguli [b,c], B.A. Cola [d], A.A. Voevodin [b]

[a] Department of Chemical and Materials Engineering, University of Dayton, Dayton, OH 45469-0240, United States
[b] Air Force Research Laboratory, Materials and Manufacturing Directorate, Thermal Sciences and Materials Branch, 2941 Hobson Way, Wright-Patterson Air Force Base, OH 45433, United States
[c] University of Dayton Research Institute, 300 College Park, Dayton, OH 45469, United States
[d] George W. Woodruff School of Mechanical Engineering and School of Materials Science and Engineering, Georgia Institute of Technology, Atlanta, 30332, United States

ARTICLE INFO

Article history:
Received 27 August 2012
Accepted 26 January 2013
Available online 1 February 2013

ABSTRACT

Vapor phase growth of gold, nickel and titanium metal nanoparticles on multiwall carbon nanotube (MWCNT) buckypaper by sputtering was investigated. The size and distribution of nanoparticles was dependent on the intrinsic binding energy of the metal elements, but could be altered to mimic that of metals with different binding energies by *in situ* modification of the MWCNT surfaces by energetic metal ions or annealing of the buckypaper. A range of average gold particle diameters from approximately 5–30 nm could be produced depending on the intrinsic sputter process parameters (especially metal ion flux and kinetic energy) and defect density of the MWCNT surfaces, which could also be controlled by annealing prior to sputtering. The diameter of the MWCNTs had a significant influence on the geometry of the nanoparticles. Particles were elongated along the nanotube axis for tube diameters <30 nm. Remarkably strong alignment of the particles along the nanotube axis was observed, especially for MWCNTs with higher defect densities.

© 2013 Elsevier Ltd. All rights reserved.

1. Introduction

Nanoparticle-decorated carbon nanotubes (CNTs) have been thoroughly investigated as chemical and biological sensors [1,2], surfaces for heterogenous catalysis [3], photovoltaics [4], tips for scanning probe microscopy [5,6] and conformal thermal or electrical contact interface materials for electronics [7–9]. The particle morphology on the CNT sidewalls strongly affects the properties and performance of metal–nanotube composites for such applications. Often nanoparticles are deposited by electrochemical methods, which generally require time consuming treatments with strong acid for surface defect production, which can result in a compromise of the intrinsic mechanical or transport properties of the CNTs, inhibiting their multifunctionality [10]. Also, the electrodeposition process is characterized by multiple parameters that are challenging to control or scale up. Moreover, electrodeposited films on CNT arrays often have high stresses, resulting in cracking on film surface [11].

We have examined physical vapor deposition techniques as scalable alternatives to electrochemical treatment for growth of metal nanoparticles on the sidewalls of multi-wall carbon nanotubes (MWCNTs) to further enable their use in applications such as those described above. Reports of nanoparticle growth on nanotubes from thermally evaporated materials were made as early as 2000, where Zhang et al. showed morphologies of different metals on single wall CNTs and discussed some aspects of metal nucleation and growth kinetics specific to the CNT substrate [12]. A recent experimental study by Scarselli et al. further highlighted the ther-

* Corresponding author.
E-mail address: cmuratore1@udayton.edu (C. Muratore).
0008-6223/$ - see front matter © 2013 Elsevier Ltd. All rights reserved.
http://dx.doi.org/10.1016/j.carbon.2013.01.074

Report Documentation Page

Form Approved
OMB No. 0704-0188

Public reporting burden for the collection of information is estimated to average 1 hour per response, including the time for reviewing instructions, searching existing data sources, gathering and maintaining the data needed, and completing and reviewing the collection of information. Send comments regarding this burden estimate or any other aspect of this collection of information, including suggestions for reducing this burden, to Washington Headquarters Services, Directorate for Information Operations and Reports, 1215 Jefferson Davis Highway, Suite 1204, Arlington VA 22202-4302. Respondents should be aware that notwithstanding any other provision of law, no person shall be subject to a penalty for failing to comply with a collection of information if it does not display a currently valid OMB control number.

1. REPORT DATE	2. REPORT TYPE	3. DATES COVERED
FEB 2013		**00-00-2013 to 00-00-2013**

4. TITLE AND SUBTITLE	5a. CONTRACT NUMBER
Nanoparticle decoration of carbon nanotubes by sputtering	5b. GRANT NUMBER
	5c. PROGRAM ELEMENT NUMBER
6. AUTHOR(S)	5d. PROJECT NUMBER
	5e. TASK NUMBER
	5f. WORK UNIT NUMBER
7. PERFORMING ORGANIZATION NAME(S) AND ADDRESS(ES) **Georgia Institute of Technology,George W. Woodruff School of Mechanical Engineering,Atlanta,GA,30332**	8. PERFORMING ORGANIZATION REPORT NUMBER
9. SPONSORING/MONITORING AGENCY NAME(S) AND ADDRESS(ES)	10. SPONSOR/MONITOR'S ACRONYM(S)
	11. SPONSOR/MONITOR'S REPORT NUMBER(S)

12. DISTRIBUTION/AVAILABILITY STATEMENT
Approved for public release; distribution unlimited

13. SUPPLEMENTARY NOTES

14. ABSTRACT

Vapor phase growth of gold, nickel and titanium metal nanoparticles on multiwall carbon nanotube (MWCNT) buckypaper by sputtering was investigated. The size and distribution of nanoparticles was dependent on the intrinsic binding energy of the metal elements but could be altered to mimic that of metals with different binding energies by in situ modification of the MWCNT surfaces by energetic metal ions or annealing of the buckypaper. A range of average gold particle diameters from approximately 5?30 nm could be produced depending on the intrinsic sputter process parameters (especially metal ion flux and kinetic energy) and defect density of the MWCNT surfaces, which could also be controlled by annealing prior to sputtering. The diameter of the MWCNTs had a significant influence on the geometry of the nanoparticles. Particles were elongated along the nanotube axis for tube diameters <30 nm. Remarkably strong alignment of the particles along the nanotube axis was observed, especially for MWCNTs with higher defect densities.

15. SUBJECT TERMS

16. SECURITY CLASSIFICATION OF:			17. LIMITATION OF ABSTRACT	18. NUMBER OF PAGES	19a. NAME OF RESPONSIBLE PERSON
a. REPORT	b. ABSTRACT	c. THIS PAGE			
unclassified	**unclassified**	**unclassified**	**Same as Report (SAR)**	**8**	

modynamics of metal–nanotube interfaces dictating particle size and morphology [13]. Their work employed thermal evaporation of different metals for nanoparticle growth, with observed changes in particle size (but not density) with deposition time. Other studies of thermally evaporated nanoparticles on nanotubes reported a weak size and areal density dependence on exposure time to metal vapor, growth temperature, or rf plasma pretreatment [14–16]. Prior studies employing sputtered noble metal films on nanotube arrays [7,11,17] identified island growth, followed by subsequent coalescence as the mechanism of growth, but focused on performance of the metallized arrays rather than processing-structure relationships. Collectively, results from the studies mentioned above indicate that the morphology of evaporated metal particles or films on individual CNTs is less dependent on process parameters than on the intrinsic properties of the metals themselves, such as their surface energy, cohesion energy, or self-diffusion activation energy, relative to the same respective values for the CNTs. Consideration of kinetic and thermodynamic models of nucleation and growth, discussed in review articles, such as Venables et al. [18] can provide insight on vapor phase process variables (some of which may not be accessible in thermal evaporation, such as ion fluxes) that can be used to alter metal nanoparticle size, shape and areal density. The Volmer–Weber model generally applies to metal particle growth on graphite where metal atoms are more strongly bound to each other than to the substrate. During Volmer–Weber growth, adatoms with sufficient kinetic energy move along the substrate surface during their lifetime to form clusters, which then act as condensation centers for other atoms. The clusters initially develop with an increase in free energy until a critical size is reached, then growth proceeds with decreasing free energy. Clusters larger than the critical size become stable, while smaller clusters remain unstable until they accumulate the necessary number of atoms. The effect of the metal cohesion energy of the deposited material on the density of nuclei is considered in the Walton relation [19]:

$$\frac{n_o}{N_o} = \left(\frac{n_1}{N_o}\right)^j \sum_m C_j(m) e^{(\beta E_j(m))} \quad \text{where } \beta = \frac{1}{\kappa T} \tag{1}$$

where the number of viable nuclei (n_o) of critical size or larger is given in terms of the growth temperature (T) and cohesive energy for the metal atom with atoms of like kind (E_j). In Eq. (1), N_o is the number of adsorption sites, k is the Boltzmann constant, m is the type of cluster (identified by crystallographic orientation), $C_j(m)$ is a statistical weight for each cluster, and n_1 is the number of clusters containing only one atom. This dependence of n_o on E_j results from the change in an incident atom's potential energy as it is reduced by a value equivalent to that of the cohesive energy when that atom is integrated into an established film nucleus. It has been shown on diverse substrates that elemental metals with higher cohesive energies of 5–7 eV (such as titanium or nickel) demonstrate higher nucleation densities than metals with lower cohesive energies of ~3 eV, such as gold, due to the magnitude of this reduction in energy [20]. Naturally, the surface energy (energy required to produce a new surface in a collection of like atoms) scales with cohesive energy, and also has a strong effect on metal morphology, as does diffusion activation energy. Comparison of the metal–graphene interfacial energy to the surface energy of the metal dictates its wetting behavior; if the interfacial energy is comparable to the surface energy, the metal will avoid contact with the substrate and form an isolated island to minimize interfacial energy. Significantly lower interfacial energy values will drive the metal to spread on the surface—for example, He et al. reported negative values of calculated interfacial energies for the (100) orientation of Ti grown on the 002 graphite surface, resulting in uniform dispersal of Ti atoms as if they were applied to a Ti surface [20]. Based on this analysis, one would expect a lower areal density of larger metal particles to evolve for metals with low binding energies and high diffusion rates. This is consistent with the reports mentioned above for thermally evaporated gold, while titanium and nickel are characterized by more conformal, layer-like thin film growth.

As mentioned above, the cohesion energy of the metal is related to its surface energy and the interfacial energy of the metal nanoparticle with CNT substrates. While the intrinsic properties of the desired metal cannot be altered, the surface energy of the nanotube substrate can, which is the purpose of acid or plasma pretreatment prior to nanoparticle growth. The relationship between defect density and nanoparticle density can be understood using thermodynamic considerations. After Venables et al. [18], a viable 3-D nuclei (a similar argument can also be made for 2-D nuclei) with the critical number of atoms (j) has a free energy ($\Delta G(j)$) that can be described by:

$$\Delta G(j) = -j\Delta\mu + j^{2/3}X \tag{2}$$

where $\Delta\mu$ is the change in chemical potential (which increases with the magnitude of the atomic metal vapor flux to substrate) and X is related to the surface energy at the metal–substrate interface:

$$X = C_m\gamma_m + C_{ms}(\gamma_{ms} - \gamma_s) \tag{3}$$

where C is related to the metal–CNT contact area and γ is the surface energy of the metal (m), substrate (s) or interface (ms). By differentiating the free energy equation, the cluster size with the maximum free energy (i, or critical cluster size) is found to be related to the free energy term, X:

$$i = \left(\frac{2X}{3\Delta\mu}\right)^3 \tag{4}$$

If the surface energy of the substrate (γ_s) can be increased (reducing the value of X) by increasing the defect density, the critical cluster size is reduced. Therefore, it is expected that nanoparticle size and density can be altered by introducing defects on the CNT surface.

In this work, effects of particle growth temperature and time on metal nanoparticle density and morphology were investigated for metals selected to represent a broad range of cohesive energies. Parameters to alter morphology for a given metal with a fixed cohesive energy, such as nanotube diameter (i.e., curvature) and CNT defect densities were investigated. Also, the energy distributions of incident metal ions and atoms were measured to evaluate their effects on nanoparticle diameter and density, as the energy of incident species was more than adequate to induce formation of defects in nanotube sidewalls, reducing the interfacial energy as discussed above.

Investigations were conducted on buckypaper substrates, made of an extruded sheet of multiwall carbon nanotubes with their growth axes generally coplanar, but rotated in essentially random directions. These substrates were especially useful for studying effects of curvature on metal nucleation and growth as they were composed of MWCNTs with a range of different diameters from ~10 to 50 nm, providing the means for a simple, combinatorial study relating curvature to metal particle morphology. Characteristics of particles grown on as received buckypaper substrates were compared to those measured on highly oriented pyrolytic graphite (HOPG) and annealed buckypaper to further evaluate effects of curvature and defect density.

2. Experimental details

All nanoparticle growth experiments were conducted in an ultra high vacuum (base pressure $<5\times10^{-9}$ Torr) processing chamber. A direct current (dc) power supply was used for sputtering metal from 3.0 cm, >99.99% pure elemental targets with power of 10–20 W in 10 mTorr ultra high purity argon. A deposition rate of approximately 1 Å s^{-1} was measured for all metals using a combination of profilometry measurements coupled with high resolution scanning electron microscopy (SEM) observations of thin film cross sections of samples deposited simultaneously on silicon wafers alongside MWCNT buckypaper substrates. Samples were mounted to an Inconel plate which was heated to the desired temperature by a thermionic filament aimed at the backside of the metal plate. The surface temperature was actively controlled via feedback from a calibrated pyrometer. To examine effects of ion flux on metal morphology, a high power impulse magnetron sputtering (HiPIMS) power supply was also used to apply multi-kilowatt pulses to the sputtering targets, but with the duty factor adjusted to provide the same average power as the dc magnetron sputtering process. The metal ion and atom energy distributions at the electrically grounded substrate were measured with a Hiden Analytical Ltd. electrostatic quadrupole plasma (EQP) analyzer, which relies on a 45° field sector analyzer for energy distribution measurement of ions of a particular mass when used in-line with a quadrupole spectrometer. Data was collected during magnetron sputtering of gold with dc and HiPIMS power supplies. The acquisition time was 200 μs for each energy increment of 0.1 eV, allowing time-averaged collection over approximately 12 pulses for each data point. Substrates were $1\times1\times0.001$ cm foils cut from the same buckypaper sheet. Additional tests were conducted on Grade 1 highly oriented pyrolitic graphite (HOPG) from SPI Inc. A Sirion high resolution (SEM) was used to observe nanoparticle morphology at high magnifications on all substrates. Analysis of electron micrographs allowed for measurement of particle size as well as areal density and morphology. To measure average particle sizes, micrographs were enlarged to enhance visibility of particles sized close to the resolution limit of the microscope and counted along 250 nm lengths MWCNTs with no less than five different diameters. A sample of buckypaper was annealed at 2500 °C for 4 h to alter the defect density, as measured by Raman spectroscopy. Transmission electron micrographs of the annealed nanotubes were compared to those in the as-received condition. Nanoparticles were grown simultaneously on annealed and unannealed buckypaper to evaluate effects of CNT defect density on nanoparticle nucleation.

3. Results

Fig. 1 shows the morphology and distribution of (a–c) gold, (d–f) nickel and (g–i) titanium nanoparticles on MWCNTs comprising the as-received buckypaper substrate. The average particle diameter increased with the deposition temperature for all metals, and decreased with reported cohesive energies associated with nanoparticle elemental composition as discussed above. The particles were relatively large for gold (up to ~24 nm), while titanium particles showed diameters of less than 5 nm and were difficult to resolve with the SEM for all processing temperatures. The areal density of particles on CNT sidewalls (Fig. 2) was related to the metal itself, as well as the processing temperature, with the gold particle density dropping nearly a factor of 10 when the temperature was increased from 150 to 300 °C. Gold and nickel nanoparticles demonstrated a clear geometry dependence on nanotube diameter, where particles were generally elongated parallel to the CNT axis. Fig. 3 indicates that the density of elongated gold particles increases with decreasing nanotube diameters by showing a count of particles along an arbitrary axial length of a nanotube of the specified diameter for the sample processed at 300 °C. For tubes of >30 nm diameter, the particles are equiaxed or elongated in axial or radial directions with essentially equivalent frequency. A better understanding of substrate curvature effects on metal morphology was desired. A 50 nm thick gold film was grown on a buckypaper and atomically flat sample of HOPG using dc sputtering at 25 °C. Particles were ~2× larger in diameter for the HOPG samples (~15 nm compared to 30 nm for the HOPG) as shown in Fig. 4.

At least two characteristics differentiate HOPG from the nanotubes: the curvature and the nature and density of the surface defects present. To better understand the role of defects on nanoparticle diameter and areal density, a sample of buckypaper was annealed in argon at 2500 °C for 4 h to reduce its defect density. Raman spectra and transmission electron micrographs of the as-received (b) and annealed (c) buckypaper samples are shown in Fig. 5. The Raman data were normalized to the 2D peak intensity. The reduction in D to G peak intensity ratio (0.05 for annealed compared to 0.28 for as-received), coupled with the increased sidewall alignment apparent in Fig. 5c indicate that annealing effectively reduced defect density.

The energy distributions of Au^+ ions measured at the substrate location with the energy analyzer/mass spectrometer for the two different magnetron sputtering processes (dc and HiPIMS) are shown in Fig. 6. Characterization of the dc magnetron sputtering discharge, with identical conditions used to process the samples shown in Fig. 1a–c, is shown in Fig. 6a. The intensity of the ion energy distribution is directly proportional to the flux of ions arriving at the substrate during nanoparticle growth. The ion flux is relatively low for the dc process, and the maximum detected ion energy was 5 eV. Fig. 6b shows the kinetic energy distributions of Au^+ ions

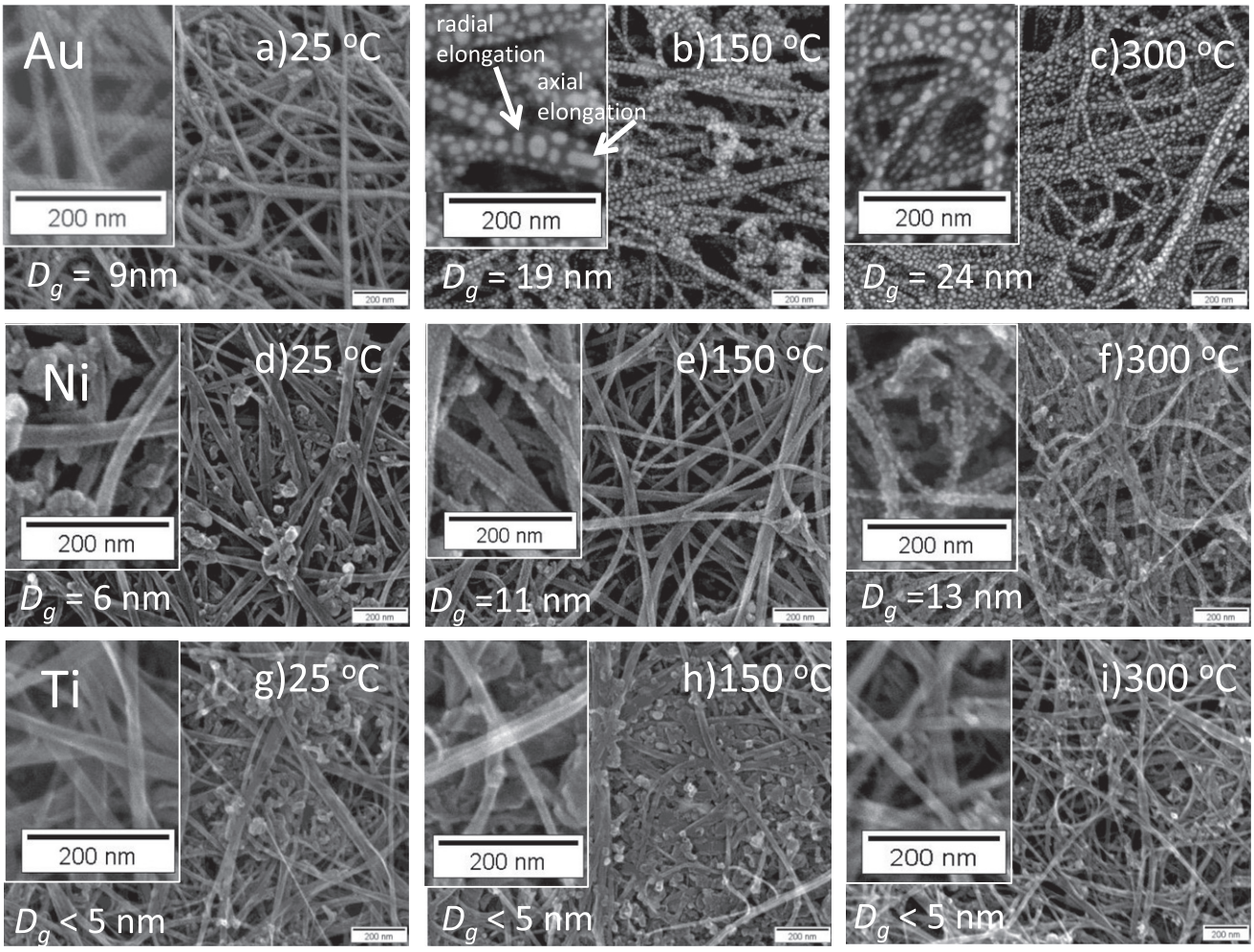

Fig. 1 – Scanning electron micrographs of buckypaper decorated with (a–c) gold, (d–f) nickel, and (g–i) titanium nanoparticles. The temperature of the buckypaper during nanoparticle growth in indicated for each micrograph.

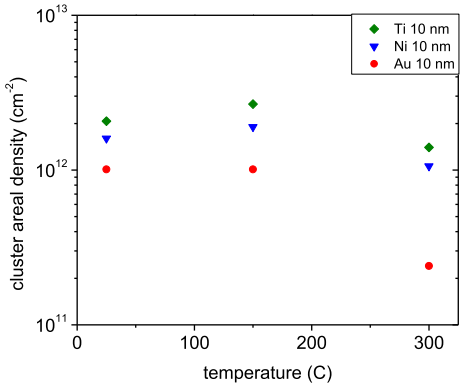

Fig. 2 – The areal density of clusters for each metal at the specified temperature.

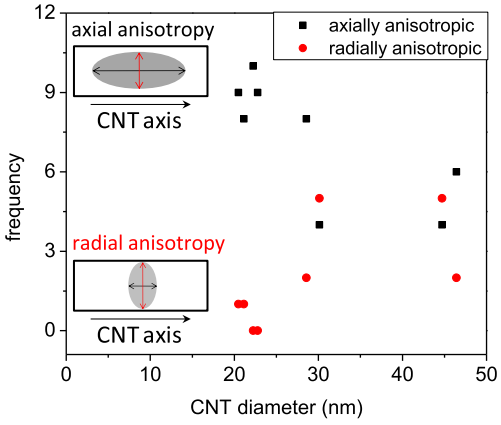

Fig. 3 – The number of particles elongated in the axial (black squares) or radial (red circles) directions along a length of approximately 250 nm along nanotubes of the specified diameter. (For interpretation of the references to color in this figure legend, the reader is referred to the web version of this article.)

arriving at the substrate when immersed in a magnetron sputtering discharge generated with high power pulses (HiP-MS) applied to the sputtering cathode at very low duty factor. The Au^+ ion flux is approximately $10^4\times$ higher and the maxi-

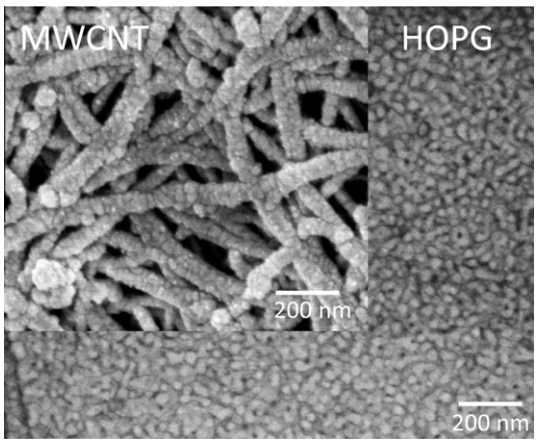

Fig. 4 – Differences in nanoparticle morphology for gold grown simultaneously on buckypaper and HOPG samples.

mum ion energy was approximately 15 eV. Nanoparticles were grown on the same samples characterized in Fig. 4 for both dc and HiPIMS processes. Fig. 7a shows gold nanoparticles grown with dc magnetron power on the annealed buckypaper substrate. The particle growth conditions were equivalent to those used to generate Fig. 1b, with the substrate at 150 °C and a nominal thickness of 3 nm. Comparison of Fig. 7a to Fig. 1b reveals that annealing results in slightly larger mean particle sizes (~30 nm compared to ~20 nm). Fig. 7b shows annealed buckypaper decorated with nanoparticles grown with the HIPIMS process at 150 °C. The average particle size is reduced to approximately 12 nm. When the particles are grown on the as-received buckypaper using the HIPIMS process at 150 °C (Fig. 7c) the particles are smaller (4 nm on average), and highly ordered along the CNT axis. The particles deposited during HIPMS processing are much less likely to show elongation along the axis than those grown using lower energy, DC sputtering. Occasionally, hexagonal patterns for the nanoparticles are clearly observed (two examples are marked on Fig. 7c). More often, partial hexagons with one or more elongated vertices are present on CNT sidewall surfaces. Fig. 7 also shows the Raman spectra of the gold nanoparticle decorated buckypaper samples. The D/G peak intensity ratio increases from left to right. DC sputtering on annealed buckypaper restored the D/G intensity ratio to approximately that of the as-received substrate.

4. Discussion

The shape, diameter and distribution of the nanoparticles differed for each metal, even when processing conditions and substrates were identical (Fig. 1). Qualitative agreement with models for nucleation density and growth kinetics was observed, where particle density increased with the cohesion energy of the metal, and particle size decreased. The drop in nanoparticle density was more pronounced for gold than for the other metals, with a significant drop at 300 °C, suggesting a different mechanism of particle coarsening. This was likely Ostwald ripening, due to the higher mobility of the gold clusters.

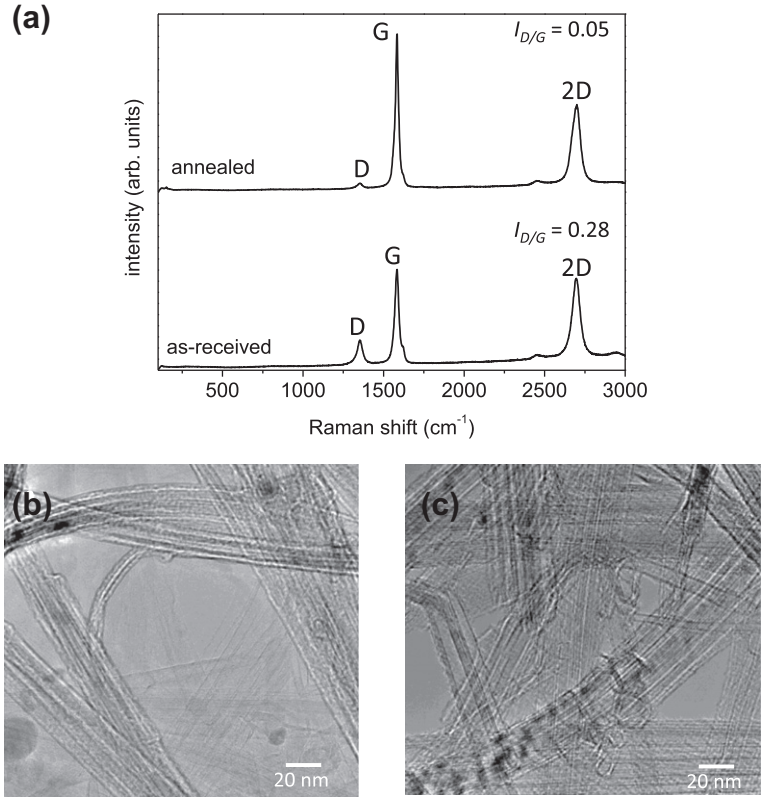

Fig. 5 – Raman spectra (a) and accompanying transmission electron micrographs for (b) as-received and (c) annealed buckypaper.

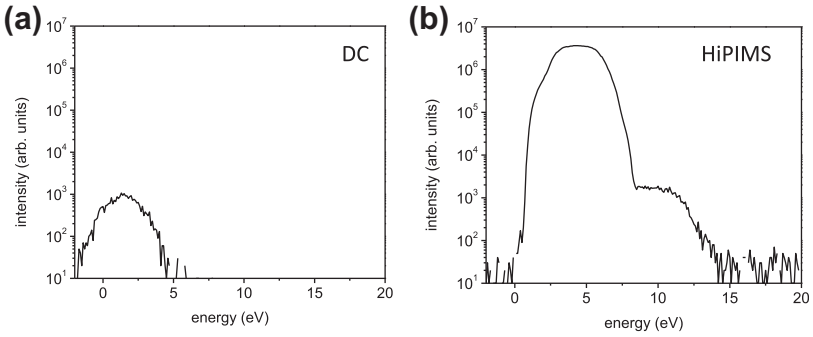

Fig. 6 – Au^+ ion energy distributions measured for (a) dc and (b) HiPIMS processing conditions.

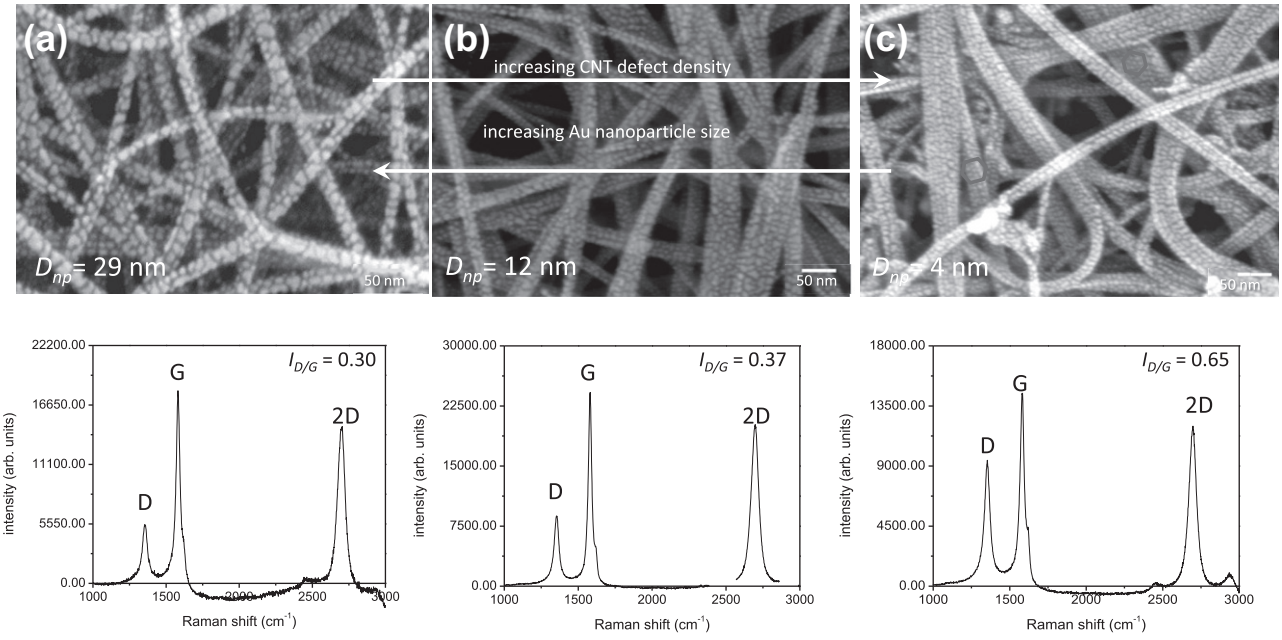

Fig. 7 – Scanning electron micrographs and accompanying Raman spectra for (a) annealed buckypaper with dc nanoparticle growth, (b) annealed buckypaper with HiPIMS growth, and (c) as-received buckypaper with HiPIMS growth. The D/G intensity ratios suggest decreasing particle size with increasing CNT defect density.

Theoretical concepts related to the observed elongation of the particles along the CNT axis for smaller diameter tubes have been discussed in the literature, and a review of prior studies on thermally evaporated gold particles seem to indicate similar morphologies, with axial elongation [12,13,15]. The molecular dynamics simulation results of Shu and Gong [21], which are also insightfully discussed by Wu et al. [22], reported that diffusion paths and barriers were strongly curvature (and chirality) dependent. They reported that atoms adsorbed on the exterior of armchair nanotubes should demonstrate weaker barriers to axial diffusion compared to radial diffusion, and related the behavior induced by positive curvature of the nanotube sidewall exterior to that shown for particles diffusing on surfaces under tensile strain. Subsequent studies based on density functional calculations by Gulseren et al. [23] relate curvature to the binding energy of foreign atoms in terms of changes in band structure (with a R^{-1} dependence), resulting in decreased mobility of adsorbed atoms during nanoparticle growth.

The activation energy for gold diffusion on nanotube sidewalls is estimated to be on the order of 0.2 eV. The lack of elongation observed for HIPIMS deposited particles (Fig. 7) is likely due to the large incident ion kinetic energy, as shown in Fig. 7b, where a large fraction of adsorbed atoms have more than enough energy to overcome the barriers associated with radial diffusion, thereby having no effect on particle morphology. The Raman spectra in Fig. 5 suggest higher metal ion fluxes and energy incident on the CNTs created defects in the substrate during nanoparticle growth, increasing the nanoparticle density as discussed in Section 1. There are conflicting reports on the relationship between D/G peak intensity ratios and defect densities. For example, Ref. [24] states that no relationship exists while Ref. [25] (cited in Ref. [24]) concludes that the D/G ratio is a reliable indicator of defect densities. The nucleation and growth phenomena we observed in this work are consistent with the increased defect densities presumably correlated to the D/G ratios we measured.

While the nanoparticles grown via sputtering demonstrate some morphological similarities to thermally evaporated particles, their axial alignment is one remarkable difference. Unlike thermal evaporation, energetic atoms deposited on CNT sidewalls by HIPIMS demonstrate sufficient mobilities to migrate to energetically favorable substrate sites. For the case of gold, this site is reported to be above the carbon atoms forming the vertices marked by the carbon atoms constituting the nanotube [26]. Based on the hexagonal patterns called out in Fig. 7c, it is assumed that alignment results from preferential cluster formation at point defects sites related atomic positions of the carbon atoms comprising the outer nanotube. Of course, the spacing between each hexagon comprising the nanotubes is much less than the mean particle spacing along the axis, however, study of the micrograph in Fig. 7c shows a few near "perfect" hexagons, and many with one or two vertices slightly misplaced, confounding the hexagonal symmetry, and hinting at the nature of particle alignment. It also may be possible to identify the chirality of the nanotubes based on the pattern of these metal nanoparticles by interpretation of the "twist" they demonstrate, which can be seen in the two decorated MWNTs with highlighted hexagons in Fig. 7c.

Finally, comparison of particle morphologies and areal densities in Fig. 7 suggests that the intrinsic limitations of metal nanoparticle morphologies on CNTs can be overcome by altering the CNT surface energy during nanoparticle deposition with the HiPIMS process. That is, as the particle sizes decrease and areal density increases, gold particles start to look more like titanium nanoparticles on the CNTs. The impact of sidewall defect densities, which are necessary to induce changes in particle characteristics, on the thermal and electrical properties of CNT–metal composite materials will be investigated in subsequent work.

5. Conclusions

Control of the areal density, diameter and morphology of metal nanoparticles grown on as-received and annealed multiwalled carbon nanotube sidewalls by sputtering was demonstrated for gold, nickel and titanium. Different metals were shown to have intrinsically different morphologies depending on their cohesion energy. Metals with larger cohesive energies exhibited a higher nanoparticle density and smaller particle diameters. Particle characteristics could be altered with temperature, total incident ion flux during processing, or by initial CNT diameters. Consistent with kinetic theory of nucleation and growth, higher nanoparticle growth temperatures increased diameter and reduced particle densities. Higher metal ion fluxes and energy incident on the CNTs created defects in the substrate during nanoparticle growth, increasing nanoparticle density. Curvature in the substrate altered the morphology of the nanoparticles, with higher densities of elongated gold particles growing on multiwalled nanotubes with a diameter of 30 nm or less. Unlike thermal evaporation, atoms deposited on CNT sidewalls by sputtering demonstrate sufficient mobilities to migrate to high energy defect sites, resulting in nanoparticle alignment along nanotube sidewalls. The extent of this alignment is reduced when the nanotubes are annealed. The process used to grow the nanoparticles is easily scalable to large arrays of CNTs, and will be explored for adding multifunctionality to CNT-based composites.

Acknowledgements

The authors would like to thank the Air Force Office of Scientific Research for funding this work under the Low Density Materials Program, Project #FA8650-09-D-5307. B.C. was supported by the Air Force Research Laboratory Summer Faculty Program. C.M. is also grateful for insightful discussions with John Taphouse, Tom Bougher, Michael Check, Shawn Putnam, John Ferguson, Tim S. Fisher, and Ajit Roy.

REFERENCES

[1] Claussen JC, Franklin AD, Haque AU, Porterfield DM, Fisher TS. Electrochemical biosensor of nanocube-augmented carbon nanotube networks. ACS Nano 2009;3:37–44.
[2] Star A, Joshi V, Skarupo S, Thomas D, Gabriel J-CP. Gas sensor array based on metal-decorated carbon nanotubes. J Phys Chem 2006;110:21014–20.
[3] Zhang H, Qiu J, Liang C, Li Z, Wang X, Wang Y, et al. A novel approach to Co/CNTs catalyst via chemical vapor deposition of organometallic compounds. Catal Lett 2005;101:211–4.
[4] Somani PR, Somani SP, Umeno M. Application of metal nanoparticle decorated carbon nanotubes in photovoltaics. Appl Phys Lett 2008;93:033315-1–3.
[5] Deng Z, Yenilmez E, Leu J, Hoffman JE, Straver EWJ. Metal-coated carbon nanotube tips for magnetic force microscopy. Appl Phys Lett 2004;85:6263.
[6] Yenilmez E, Zhang H, Zhang L, Deng Z, Moler KA. Pattern-free growth of carbon nanotube tips for scanning probe microscopy. Nanosci Nanotechnol Lett 2011;3:669–73.
[7] Bult J, Sawyer WG, Voevodin AA, Muratore C, Dickrell P, Pal S, et al. Electrical switching using compliant metal infiltrated multi-wall nanotube arrays. MRS Proc 2008;1085. 1085-T02–1085-T05.
[8] Cross R, Cola BA, Fisher TS, Xu X, Gall K, Graham S. A metallization and bonding approach for high performance carbon nanotube thermal interface materials. Nanotechnology 2010;21:445705-1–8.
[9] Panzer MA, Zhang G, Mann D, Hu X, Pop E, Dai H, et al. Thermal properties of metal-coated vertically aligned single-wall nanotube arrays. J Heat Trans 2008;130:052401-1–9.
[10] Wildgoose GG, Banks CE, Compton RG. Metal nanoparticles and related materials supported on carbon nanotubes: methods and applications. Small 2006;2:182–93.
[11] Yaglioglu O, Martens R, Cao A, Slocum AH. Compliant carbon nanotube-metal contact structures. In: IEEE 57th holm conference on electric contacts; 2011 [978-1-61284-651-4/11].
[12] Zhang Y, Franklin NW, Chen RJ, Dai H. Metal coating on suspended carbon nanotubes and its implication to metal–tube interaction. Chem Phys Lett 2000;331:35–41.
[13] Scarselli M, Camilli L, Castrucci P, Nanni F, Del Gobbo S, Gautron E, et al. In situ formation of noble metal nanoparticles on multiwalled carbon nanotubes and its implication in metal–nanotube interactions. Carbon 2012;50:875–84.
[14] Bittencourt C, Ke X, Van Tendeloo G, Thiess S, Drube W, Ghijsen J, et al. Study of the interaction between copper and carbon nantoubes. Chem Phys Lett 2012;535:80–3.
[15] Gingery D, Buhlmann P. Formation of gold nanoparticles on multiwalled carbon nanotubes by thermal evaporation. Carbon 2008;46:1966–72.

[16] Charlier J-C, Arnaud L, Avilov IV, Delgado M, Demoisson F, Espinosa EH, et al. Carbon nanotubes randomly decorated with gold clusters: from nano2hybrid atomic structures to gas sensing prototypes. Nanotechnology 2009;20:375501–11.
[17] O. Yaglioglu, Thesis. Massachusetts Institute of Technology, Department of Mechanical Engineering; 2007.
[18] Venables JA, Spiller GDT, Hanbucken M. Nucleation and growth of thin films. Rep Prog Phys 1984;47:399–458.
[19] Walton D. Nucleation of vapor deposits. J Chem Phys 1962;37:2182–8.
[20] He Y, Zhang J, Wang Y, Yu Z. Coating geometries of metals on single-walled carbon nanotubes. Appl Phys Lett 2010;96:063108-1–3.
[21] Shu DJ, Gong XG. Curvature effects on surface diffusion: the nanotube. J Chem Phys 2001;124:10922–5.
[22] Wu M-C, Li C-L, Hu C-K, Chang Y-C, Liaw Y-H, Huang L-W, et al. Curvature effect on the surface diffusion of silver adatoms on carbon nanotubes: deposition experiments and numerical simulations. Phys Rev B 2006;74:125424-1–8.
[23] Gulseren O, Yildirim T, Ciraci S. Tunable adsorption on carbon nanotubes. Phys Rev Lett 2001;87:116802-1–4.
[24] Lehman JH, Terrones M, Mansfield E, Hurst KE, Meunier V. Evaluating the characteristics of multiwall carbon nanotubes. Carbon 2011;49:2581–602.
[25] Osswald S, Flahaut E, Ye H, Gogotsi Y. Elimination of D-band in Raman spectra of double-wall carbon nanotubes by oxidation. Chem Phys Lett 2005;402:422–7.
[26] Dag S, Gulseren O, Yildirim T, Ciraci S. Oxygenation of carbon nanotubes: atomic structure, energetics and electronic structure. Phys Rev B 2003;67:165424.